Advances in Differential Equations and Control Processes 2026, 33(2), 2805.
https://doi.org/10.59400/adecp2805

Article

A novel mean curvature-based model for positive image restoration and blur kernel estimation in blind image deblurring

Azhar Iqbal[1], Shahid Saleem[2], Shahbaz Ahmad[1], Adel M. Al-Mahdi[3,*], Faisal Fairag[3]

[1] Abdus Salam School of Mathematical Sciences (ASSMS), Government College University, Lahore 54000, Pakistan

[2] Department of Mathematics, The University of Chenab, Gujrat 50700, Pakistan

[3] Department of Mathematics, King Fahd University of Petroleum & Minerals, Dhahran 31261, Saudi Arabia

*** Corresponding author:** Adel M. Al-Mahdi, almahdi@kfupm.edu.sa

CITATION

Iqbal A, Saleem S, Ahmad S, et al. A novel mean curvature-based model for positive image restoration and blur kernel estimation in blind image deblurring. Advances in Differential Equations and Control Processes. 2026; 33(2): 2805. https://doi.org/10.59400/adecp2805

ARTICLE INFO

Received: 17 February 2025
Revised: 20 December 2025
Accepted: 26 December 2025
Available online: 20 May 2026

Abstract: The premise of blind image deblurring revolves around the restoration of a clear image from a blurred one without prior knowledge of the specific blur kernel employed. Within this realm, various image priors have been extensively investigated and applied to address this inherently challenging problem. Throughout the image deblurring process, ensuring the resulting image intensities remain strictly non-negative is often imperative. However, prevalent numerical methodologies utilized to solve this issue have shown instances where the outcomes are not consistently favorable, leading to undesirable negative intensities that contribute to significant areas of darkness in the restored images. This study introduces a novel model designed to tackle the blind image deblurring problem by leveraging mean curvature. The proposed model not only assures positive outcomes but also confines the upper limit of image intensity values, thereby maintaining them within a predefined range. Additionally, new numerical algorithms are introduced, which not only restore the image but also estimate the blur kernel. Comparative analyses between these proposed algorithms and existing numerical techniques have been conducted to showcase the effectiveness and feasibility of our suggested approach.

Keywords: blind image deblurring; ill-posed problem; mean curvature; constrained problem; augmented Lagrangian method

1. Introduction

In recent years, the proliferation of digital imaging devices, such as smartphones and high-resolution cameras, has made capturing images an everyday activity for millions of people worldwide. However, the inherent limitations of these devices, including camera shake, motion blur, and out-of-focus captures, often result in degraded image quality. These types of blur can significantly impact the visual content, making it challenging to interpret the image or extract relevant information. Blurring typically arises from translation or relative rotation between objects and cameras throughout the camera lens exposure duration. The mathematical relationship between original or true image u and blurry image z is:

$$z = \mathbf{K}u + \epsilon, \tag{1}$$

where ε represents a noise function and $\mathbf{K}$ represents of blurring operator;

$$(\mathbf{K}u)(x) = \int_{\Omega} k(x,y)u(y)\,dy, \quad \mathbf{x} \in \Omega. \tag{2}$$

The kernel, denoted as $k(x, y) = k(x - y)$, is commonly named as a translate-invariant kernel. The $\mathbf{K}$ is a compact operator (Fredholm integral of first kind). The objective is to extract both blur kernel $\mathbf{K}$ and latent image u from the given equation. The ill-posed nature of this problem arises from the fact that multiple pairs of u and $\mathbf{K}$ can yield the same outcome z. The situation where the blurring operator $\mathbf{K}$ is known corresponds to non-blind deconvolution [1–5]. Furthermore, when the blurring operator $\mathbf{K}$ is not known, the process is recognized as the blind deconvolution [6–8].

Image deblurring techniques aim to restore the sharpness and details lost during the blurring process, providing a clearer representation of the scene. Traditional approaches to deblurring relied on assumptions about the blur kernel, such as uniform motion blur or Gaussian blur, enabling the estimation and subsequent removal of the blur effect. However, in real-world scenarios, obtaining precise knowledge about the blur kernel is often challenging or even impossible, limiting the effectiveness of these approaches. Blind image deblurring tackles the problem of restoring blurred images without any prior knowledge about the blur kernel. This branch of image deblurring has gained significant attention from researchers and practitioners due to its potential to address real-world scenarios, where the blur characteristics are unknown or highly complex. The aim is to develop algorithms that can autonomously estimate the blur kernel and perform image restoration simultaneously, effectively addressing both the inherent blur and the lack of knowledge about it.

The use of energy minimization models [9–12] for the solution of the image deblurring problem has gained significant attention and interest in recent decades.

$$\min_{u \in C} \int_{\Omega} (k * u - z)^2 d\Omega + \alpha R(u) \tag{3}$$

In the given expression, C denotes the constrained set, $R(u)$ is the regularization functional, and $\alpha > 0$ serves as a parameter of regularization. This parameter plays a crucial role in determining the balance between the first term (data fitting term) and the second term (regularization term) in the formulation. When employing these methods on photos affected by noise and blur, researchers encounter two prominent challenges that need to be addressed. The primary challenge involves dealing with non-linearity, while the secondary challenge revolves around resolving massive matrix systems at play. The Total variation (TV)-based blind deconvolution model [13–15] is defined as

$$\min_{u} \int_{\Omega} (k * u - z)^2 \, d\Omega + \alpha_1 \|u\|_{TV,\beta} + \alpha_2 \|k\|_{TV,\beta} \tag{4}$$

such that:

$$u \geq 0, \quad k \geq 0, \tag{5}$$

$$\int_{\Omega} k(s, t) \, ds \, dt = 1, \quad k(x, y) = k(-x, -y), \tag{6}$$

here $\|w\|_{TV,\beta} = \int_{\Omega} |\bigtriangledown w|_{\beta} d\Omega$, $|\bigtriangledown w|_{\beta} = \sqrt{w_x^2 + w_y^2 + \beta}$. In this context, the parameter $\beta > 0$ is employed to ensure that the functional $\|w\|_{TV,\beta}$ becomes differentiable at zero. The positive parameters α_1 and α_2 balance between good fit and regularity of the solutions u and k. There is no proof that guarantees uniqueness of the solutions [15]

in practice of Equations (4)–(6) produces good solutions. The TV model has a lot of great features, but it has one major flaw. It facilitates the transformation of piecewise constant functions into smooth ones which create staircase effects in restored images. As a consequence of the restoration process, the resulting photos might exhibit a blocky appearance. Using mean curvature (MC)-based regularisation models [16, 17] is one way to lessen the staircase impacts in restored images. The MC-based blind image deblurring model is:

$$\min_{u} \int_{\Omega} (k * u - z)^2 d\Omega + \alpha_1 \|u\|_{MC,\beta} + \alpha_2 \|k\|_{MC,\beta} \tag{7}$$

such that:

$$u \geq 0, k \geq 0,$$

$$\int_{\Omega} k(s,t) ds dt = 1, k(x,y) = k(-x,-y),$$

here $\|w\|_{MC,\beta} = \int_{\Omega} \left(\bigtriangledown \cdot \frac{\bigtriangledown w}{|\bigtriangledown w|_{\beta}} \right)^2 d\Omega$. MC-based regularization models are particularly efficient. While removing the staircase effect. In restored images, these models retain the edges. To illustrate the frequency-domain behavior of different regularizers, we provide an attenuation plot (**Figure 1**), which compares TV and our MC regularizer in terms of their effect on different frequency components.

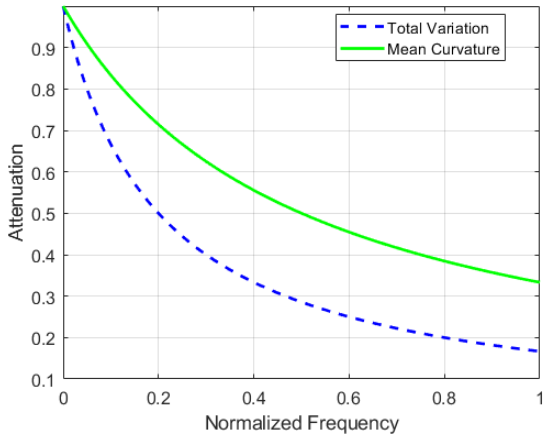

Figure 1. Attenuation graph of TV and MC.

The attenuation plot in **Figure 1** demonstrates the frequency-domain characteristics of the TV and MC regularizers. While TV exhibits strong suppression of high-frequency components, it can also over-penalize fine details, leading to loss of texture and over-smoothing. In contrast, the MC regularizer applies gentler attenuation across the spectrum, particularly at higher frequencies. This behavior allows MC to achieve a better trade-off between noise reduction and detail preservation, enabling reconstructions that maintain fine-scale structures while still providing effective regularization.

Especially in the context of astronomical imaging, when performing image deblurring, it is crucial that the restored image maintains intensity values that are strictly non-negative to ensure accurate and reliable astronomical analysis [18–22]. However, observations have highlighted that employing current techniques might yield outcomes

that are not consistently desirable. Images characterized by numerous pixels whose intensity values are close to or equal to zero are often termed as images having negative intensities or referred to as containing black spaces. This article presents the model for mean curvature-based blind image deblurring, ensuring that the resulting image intensities are strictly positive. Furthermore, the proposed model imposes constraints on the upper limit of the values of image intensity, ensuring their confinement within a predetermined range. The main goal of this paper revolves around transforming the problem of image deblurring constrained by mean curvature into an unconstrained form. To achieve this, we proposed augmented Lagrangian methods. Augmented Lagrangian methods have demonstrated successful resolution of optimization problems within the domains of image processing and computer vision [23–25]. In these works, augmented Lagrangian methods outperform other numerical techniques in terms of speed. Studies have shown that employing augmented Lagrangian methods enables the decomposition of the original complex minimization problem into several simpler and efficiently solvable sub-problems. Some of them possess solutions in closed forms, while others can be rapidly resolved by utilising tools like the fast Fourier transform (FFT). New numerical algorithms are described that not only restore the image but also estimate the blur kernel.

The paper introduces several notable contributions, which can be summarized as follows: Firstly, a modified blind image deblurring model is presented, incorporating a constraint that limits image intensity values to a predetermined range. Secondly, a novel algorithm is proposed for effectively deblurring the blurred image. Thirdly, a new algorithm is introduced to estimate the blur kernel accurately. Lastly, the theoretical findings are rigorously verified through numerical implementation. The remainder of the document is divided into sections. The modified image deblurring model is covered in the second section. The kernel minimization problem and image minimization problem are also covered in the second section. The third section presents cell discretization. The third section introduces the matrix system. The numerical experiments for our proposed approaches are detailed in the fourth section of the paper. In the final section, conclusive remarks and insights are provided on the proposed methods.

2. Modified blind deconvolution model

Blind deconvolution is the scenario when both the convolution kernel and the image itself are unknown. Here we present the modified blind deconvolution model. We address scenarios where the pixel values in digital images must be constrained to a specified interval $[a_1, a_2]$. For instance, in 8-bit images, we have $[a_1, a_2] = [0, 255]$. So MC-based modified blind deconvolution model [26–29] is described as

$$\min_u \int_\Omega (k * u - z)^2 d\Omega + \alpha_1 \|u\|_{MC,\beta} + \alpha_2 \|k\|_{MC,\beta}$$

such that:

$$a_1 \leq u \leq a_2, k \geq 0, \tag{8}$$

$$\int_\Omega k(s,t) ds dt = 1, k(x,y) = k(-x,-y).$$

Here the positive parameters α_1 and α_2 serve to balance the trade-off between achieving a good fit for data and ensuring the smoothness or regularity of obtained solutions u and k. If we ignore the upper boundary a_2, this is a classic blind deconvolution model which we have explained above. In classic blind deconvolution model, we only require strictly positive results for our image variable u.

We can minimize the functional in Equations (6)–(8) by first picking initial guess $u^{(0)}$ and resolving it for $k^{(0)}$ and then utilizing $k^{(0)}$ calculate the $u^{(1)}$ and carry out the procedure again. Therefore, knowing $u^{(n)}$ and $k^{(n)}$ algorithm is explained as:

- Kernel minimization problem: resolve it for $k^{(n+1)}$

$$\min_{k^{(n+1)}} \int_\Omega (u^{(n)} * k^{(n+1)} - z)^2 d\Omega + \alpha_2 \parallel k^{(n+1)} \parallel_{MC,\,\beta} \tag{9}$$

such that:

$$k^{(n+1)} \geq 0, \int_\Omega k^{(n+1)}(s,t)\, ds\, dt = 1, \tag{10}$$

$$k^{(n+1)}(x,y) = k^{(n+1)}(-x,-y) \tag{11}$$

- Image minimization problem: resolve it for $u^{(n+1)}$

$$\min_{u^{(n+1)}} \int_\Omega (k^{(n+1)} * u^{(n+1)} - z)^2 d\Omega + \alpha_1 \parallel u^{(n+1)} \parallel_{MC,\,\beta} \tag{12}$$

such that:

$$a_1 \leq u^{(n+1)} \leq a_2 \tag{13}$$

Now our main objective is to solve the above two problems. First we explain the kernel minimization problem and later image minimization problem.

2.1. Kernel minimization problem

In Equations (9)–(11), we have used the equality $k * u = u * k$. The augmented Lagrangian functional for Equations (9)–(11) is established for the positive penalty parameter $c > 0$ and the multipliers $\lambda_1, \lambda_2, \lambda_3$ by

$$F_c(k,\gamma,\lambda_1,\lambda_2,\lambda_3) = \int_\Omega (u * k - z)^2 d\Omega + \alpha_2 \|k\|_{MC,\beta} \tag{14}$$

$$+ \int_\Omega \lambda_1(-k+\gamma^2)d\Omega + \int_\Omega \lambda_2(k - \frac{1}{|\Omega|})d\Omega + \int_\Omega \lambda_3(k(x,y) - k(-x,-y))d\Omega$$

$$+ \frac{c}{2}\int_\Omega \left\{(-k+\gamma^2)^2 + (k - \frac{1}{|\Omega|})^2 + (k(x,y) - k(-x,-y))^2\right\} d\Omega.$$

So the Euler-Lagrange equations for k takes the following form:

$$K^*Ku + \alpha_2 \bigtriangledown .(\frac{\bigtriangledown \kappa}{\sqrt{|\bigtriangledown k|^2 + \beta^2}} - \frac{\bigtriangledown \kappa . \bigtriangledown k}{(\sqrt{|\bigtriangledown k|^2 + \beta^2})^3} \bigtriangledown k) + ck = K^*z, \tag{15}$$

where $\kappa = \bigtriangledown . \frac{\bigtriangledown k}{|\bigtriangledown k|_\beta}$ and K having adjoint operator is K^* . The Equation (15) is a fourth-order non-linear differential equation.

In terms of γ, the minimization is equal to

$$\min_{w>0}\left\{\int_{\Omega}\left[\lambda_1(-k+w)+\frac{1}{2}c(-k+w)^2\right]d\Omega\right\}. \tag{16}$$

Hence, the solution of Equation (14) is

$$w^* = \max\{\ 0,\ k-\lambda_1/c\ \}. \tag{17}$$

The multiplier technique can be explained in the following way: The given multipliers are $\lambda_1^{(n)}, \lambda_2^{(n)}, \lambda_3^{(n)}$, and $c^{(n)}$ is a penalty parameter. We use to minimize $F_{c^{(n)}}$ by getting $k^{(n)}$ and $\gamma^{(n)}$ then we set

$$\lambda_1^{(n+1)} = \lambda_1^{(n)} + c^{(n)}\max\{-k^{(n)}, \lambda_1^{(n)}/c^{(n)}\} \tag{18}$$

$$\lambda_2^{(n+1)} = \lambda_2^{(n)} + c^{(n)}(k^{(n)} - \frac{1}{|\ \Omega\ |}) \tag{19}$$

$$\lambda_3^{(n+1)} = \lambda_3^{(n)} + c^{(n)}(k(x,y) - k(-x,-y)). \tag{20}$$

To minimize the functional Equation (14), the initial step involves selecting the value of c and the function λ_1. Subsequently, we calculate w^* using the Equation (17) then we pick a function λ_2 and λ_3 and we compute u by using Equation (15). This suggests the **Algorithm 1** for Equations (9)–(11):

Algorithm 1 Kernel Minimization Method

function: $[k]$ = MinimizeK $(c, \lambda_1, \lambda_2, \lambda_3, \alpha_2, k, u)$

1. **Set:** $c^{(0)} = c, \lambda_1^{(0)} = \lambda_1, \lambda_2^{(0)} = \lambda_2, \lambda_3^{(0)} = \lambda_3, k^{(0)} = k$
2. **Set:** $w^{(0)} = \max\{0, k^{(0)} - \lambda_1^{(0)}/c^{(0)}\}$
3. For $m = 1, 2, \cdots$ **Find** $k^{(n)}$: $\min_k F_{c^{(n-1)}}(\alpha_2, k, \sqrt{w^{(n-1)}}, \lambda_1^{(n-1)}, \lambda_2^{(n-1)}, \lambda_3^{(n-1)})$
4. **Set:** $\lambda_1^{(n)} = \lambda_1^{(n-1)} + c^{(n-1)}\max\{-k^{(n-1)}, \lambda_1^{(n-1)}/c^{(n-1)}\}$
5. **Set:** $\lambda_2^{(n)} = \lambda_2^{(n-1)} + c^{(n-1)}(k^{(n-1)} - \frac{1}{|\Omega|})$
6. **Set:** $\lambda_3^{(n)} = \lambda_3^{(n-1)} + c^{(n-1)}(k(x,y) - k(-x,-y))$
7. **Test:** *Stopping criteria*
8. **Set:** $c^{(n)} = d * c^{(n-1)}$
9. **Set:** $w^{(n)} = \max\{0, k^{(n)} - \lambda_1^{(n)}/c^{(n)}\}$
10. end
11. **Set:** $k = k^{(n)}$

2.2. Image minimization problem

Now consider our image minimization Equations (12) and (13) without superscript:

$$\min_u \int_{\Omega}(k*u-z)^2 d\Omega + \alpha_1\|u\|_{MC,\ \beta} \tag{21}$$

subject to:

$$a_1 \le u \le a_2 \tag{22}$$

Initially, we transform the Equation (22) into two separate equalities

$$-u + a_1 + \gamma_1^2 = 0, \qquad u - a_2 + \gamma_2^2 = 0. \tag{23}$$

Now the Equations (21) and (22) become

$$\min_u \int_\Omega (k * u - z)^2 d\Omega + \alpha_1 \|u\|_{MC,\beta}$$

subject to:

$$-u + a_1 + \gamma_1^2 = 0, \qquad u - a_2 + \gamma_2^2 = 0.$$

Let's consider augmented Lagrangian functional associated with the Equations (21) and (23) describing the given problem where we introduce the positive penalty parameter $(c > 0)$ and associated multipliers λ_1, λ_2 by

$$\begin{aligned} G_c(u, \gamma_1, \gamma_2, \lambda_1, \lambda_2) = \int_\Omega (k * u - z)^2 d\Omega + \alpha_1 \|u\|_{MC,\beta} + \int_\Omega \lambda_1(-u + a_1 + \gamma_1^2) d\Omega \\ + \int_\Omega \lambda_2(u - a_2 + \gamma_2^2) d\Omega + \frac{c}{2} \int_\Omega \left\{(-u + a_1 + \gamma_1^2)^2 + (u - a_2 + \gamma_2^2)^2\right\} d\Omega \end{aligned} \tag{24}$$

From Equation (24), Euler Lagrange equations for u takes the following form:

$$K^*Ku + \alpha_1 \bigtriangledown .(\frac{\bigtriangledown \kappa}{\sqrt{|\bigtriangledown u|^2 + \beta^2}} - \frac{\bigtriangledown \kappa . \bigtriangledown u}{(\sqrt{|\bigtriangledown u|^2 + \beta^2})^3} \bigtriangledown u) + cu = K^*z, \tag{25}$$

where $\kappa = \bigtriangledown . \frac{\bigtriangledown u}{|\bigtriangledown u|_\beta}$ and K having adjoint operator K^*. The Equation (25) is also a non-linear fourth-order differential equation.

Now, the objective is to minimize the augmented Lagrangian of Equation (24) with respect to (u, γ_1, γ_2) for the different λ_1, λ_2, and c. Direct determination of the explicit minimization of G_c concerning γ_1 and γ_2 by fixing each u is feasible and minimization concerning γ_1 and γ_2 is defined as

$$\min_{w_1 > 0} \left\{ \int_\Omega \left[\lambda(-u + a_1 + w_1) + \frac{1}{2} c(-u + a_1 + w_1)^2 \right] d\Omega \right\} \tag{26}$$

$$\min_{w_2 > 0} \left\{ \int_\Omega \left[\lambda(u - a_2 + w_2) + \frac{1}{2} c(u - a_2 + w_2)^2 \right] d\Omega \right\} \tag{27}$$

Hence, the solutions of Equations (26) and (27) are

$$w_1^* = \max\{0,\ u - \lambda_1/c - a_1\}, \tag{28}$$

$$w_2^* = \max\{0,\ -u - \lambda_2/c + a_2\}. \tag{29}$$

Now, the multiplier method can be explained in the following way: $\lambda_1^{(n)}, \lambda_2^{(n)}$ are known multipliers and $c^{(n)}$ is a penalty parameter , we minimize the $G_{c^{(n)}}$ by getting $u^{(n)}, \gamma_1^{(n)}$ and $\gamma_2^{(n)}$ then we set

$$\lambda_1^{(n+1)} = \lambda_1^{(n)} + c^{(n)} \max\{-u^{(n)},\ -\lambda_1^{(n)}/c^{(n)} - a_1\} \tag{30}$$

$$\lambda_2^{(n+1)} = \lambda_2^{(n)} + c^{(n)} \max\{u^{(n)},\ -\lambda_2^{(n)}/c^{(n)} + a_2\} \tag{31}$$

For the minimization of the functional Equation (24), initially select the value of c and the function λ_1. Subsequently, w_1^* is computed using Equation (28). Following this, a function λ_2 is chosen and w_2^* is computed using Equation (29). Next, u is computed by using Equation (25). This is detailed in **Algorithm 2**.

Algorithm 2 Image Minimization Method

function: [u] = MinimizeU($c, \lambda_1, \lambda_2, \alpha_1, u, k$)

Set: $c^{(0)} = c, \lambda_1^{(0)} = \lambda_1, \lambda_2^{(0)} = \lambda_2$
Set: $u^{(0)} = u$
Set: $w_1^{(0)} = \max\{0, u^{(0)} - \lambda_1^{(0)}/c^{(0)} - a_1\}$
Set: $w_2^{(0)} = \max\{0, -u^{(0)} - \lambda_2^{(0)}/c^{(0)} + a_2\}$
For $m = 1, 2, \cdots$
    Find $u^{(n)}$: $\min_u G_{c^{(n-1)}}(\alpha_1, u, \sqrt{w_1^{(n-1)}}, \sqrt{w_2^{(n-1)}}, \lambda_1^{(n-1)}, \lambda_2^{(n-1)})$
    Set: $\lambda_1^{(n)} = \lambda_1^{(n-1)} + c^{(n-1)} \max\{-u^{(n-1)}, -\lambda_1^{(n-1)}/c^{(n-1)} - a_1\}$
    Set: $\lambda_2^{(n)} = \lambda_2^{(n-1)} + c^{(n-1)} \max\{u^{(n-1)}, -\lambda_2^{(n-1)}/c^{(n-1)} + a_2\}$
    Test: *Stopping criteria*
    Set: $c^{(n)} = d * c^{(n-1)}$
    Set: $w_1^{(n)} = \max\{0, u^{(n-1)} - \lambda_1^{(n-1)}/c^{(n-1)} - a_1\}$
    Set: $w_2^{(n)} = \max\{0, -u^{(n-1)} - \lambda_2^{(n-1)}/c^{(n-1)} + a_2\}$
end
Set: $u = u^{(n)}$

Therefore, our modified blind deconvolution (MBD) method on a blurry image without knowing the blurry operator or with some partial information of the blurry operator can be described in the **Algorithm 3**.

Algorithm 3 Modified Blind Deconvolution Method

function: [u, k] = Blind Deconvolution ($c, \lambda_1, \lambda_2, \lambda_3, \hat{c}, \hat{\lambda}_1, \hat{\lambda}_2, \alpha_1, u, \alpha_2, k$)

Set: $k^{(0)} = k, u^{(0)} = u$
For $m = 1, 2, \cdots$
    [$k^{(n)}$] = MinimizeK ($c, \lambda_1, \lambda_2, \lambda_3, \alpha_2, k^{(n-1)}, u^{(n-1)}$)
    [$u^{(n)}$] = MinimizeU($\hat{c}, \hat{\lambda}_1, \hat{\lambda}_2, \alpha_1, u^{(n-1)}, k^{(n)}$)
    Test: *Stopping criteria*
end
Set: $u = u^{(n)}, k = k^{(n)}$

3. Cell discretization

Due to the non-homogeneous nature of the MC regularizer κ in the image deblurring problem, it becomes necessary to employ a spatial discretization approach, particularly for terms involving derivatives. This is crucial as the spatial mesh size significantly affects numerical results for MC model. Consequently, we divided domain $\Omega = (0, 1) \times (0, 1)$ into smaller subdomains of size $\delta_x \times \delta_y$. Furthermore,

$$\delta_x : 0 = x_{1/2} < x_{3/2} < ... < x_{n_x+1/2} = 1,$$
$$\delta_y : 0 = y_{1/2} < y_{3/2} < ... < y_{n_x+1/2} = 1.$$

In this context, n_x dnotes the count of uniformly spaced partitions along x or y direction, and (x_i, y_j) corresponds to the cell centers within these partitions. Additionally,

$$x_i = \frac{(2ih - h)}{2} \quad \text{for} \quad i = 1, 2, 3, ..., n_x,$$

$$y_j = \frac{(2jh - h)}{2} \quad \text{for} \quad j = 1, 2, 3, ..., n_x,$$

here $h = \frac{1}{n_x}$. The $(x_{i\pm\frac{1}{2}}, y_j)$ and $(x_i, y_{j\pm\frac{1}{2}})$ denotes the mid-points of cell edges:

$$x_{i\pm\frac{1}{2}} = x_i \pm \frac{h}{2} \quad \text{for} \quad i = 1, 2, 3, ..., n_x,$$

$$y_{j\pm\frac{1}{2}} = y_j \pm \frac{h}{2} \quad \text{for} \quad j = 1, 2, 3, ..., n_x.$$

For each $i = 1, 2, ..., n_x$ and $j = 1, 2, ..., n_x$, we state

$$\Omega_{i,j} = (x_{i-1/2}, x_{i+1/2}) \times (y_{j-1/2}, y_{j+1/2}).$$

Let $\theta(x, y)$ be a function, and we denote $\theta_{k,l}$ as $\theta(x_l, y_m)$, here k and l can assume values of the $i - 1, i$, or $i + 1$ and $j - 1, j$, or $j + 1$, correspondingly. Here, i and j represent integers that are greater or equal to zero. In order to calculate forward and backward discrete functions, we require values at specific discrete points. To address this, we introduce the following functions for the purpose of defining these points appropriately.

$$[d_x^+\theta]_{i,j} = \frac{\theta_{i+1,j} - \theta_{i,j}}{h}, \quad [d_x^-\theta]_{i,j} = \frac{\theta_{i,j} - \theta_{i-1,j}}{h},$$
$$[d_y^+\theta]_{i,j} = \frac{\theta_{i,j+1} - \theta_{i,j}}{h}, \quad [d_y^-\theta]_{i,j} = \frac{\theta_{i,j} - \theta_{i,j-1}}{h}.$$

Subsequently, we obtain the discrete functions for central differences, denoted as:

$$[d_x^c\theta]_{i,j} = \frac{[d_x^-\theta]_{i,j} + [d_x^+\theta]_{i,j}}{2}, \quad [d_y^c\theta]_{i,j} = \frac{[d_y^-\theta]_{i,j} + [d_y^+\theta]_{i,j}}{2},$$

and the discrete gradient, denoted as:

$$[\bigtriangledown^+\theta]_{i,j} = \langle [d_x^+\theta]_{i,j}, [d_y^+\theta]_{i,j} \rangle, \quad [\bigtriangledown^-\theta]_{i,j} = \langle [d_x^-\theta]_{i,j}, [d_y^-\theta]_{i,j} \rangle.$$

Utilizing the midpoint quadrature approximation, we can express the equation as follows:

$$(Ku)(x_i, y_j) \cong [K_h U]_{(ij)}.$$

3.1. Discretization of kernel minimization problem

The CCFD approximations $\{U_{i,j}\}$ to $\{u(x_{i,j})\}$ and $\{K_{i,j}\}$ to $\{k(x_{i,j})\}$ are chosen. So from Equation (15), we have

$$[K^*KU]_{i,j} + \alpha[div^-(\frac{\bigtriangledown^+\kappa}{\sqrt{[\bigtriangledown^+K]_{i,j}^2 + \beta^2}} - \frac{\bigtriangledown^+\kappa.\bigtriangledown^+ K}{(\sqrt{[\bigtriangledown^+K]_{i,j}^2 + \beta^2})^3} \bigtriangledown^+ K)]_{i,j} + cK_{i,j} \\ = [K^*Z]_{i,j}. \tag{32}$$

By using lexicographical ordering of the unknowns, $U = [U_{11} \quad U_{12} \quad ... \quad U_{n_x n_x}]^t$ and $K = [K_{11} \quad K_{12} \quad ... \quad K_{n_x n_x}]^t$, from Equation (32), we have the following matrix system:

$$K_h^* K_h U + \alpha_2 (B_h^* D_h^{-1}(K) B_h)^2 K + \alpha_2 B_h^* D_h^{-1}(K) G_h(K) D_h^{-1} B_h K + cK = K_h^* Z. \quad (33)$$

In this case, the matrix K_h has dimensions $n_x^2 \times n_x^2$, while B_h has dimensions $2n_x(n_x-1) \times n_x^2$. The matrices G_h and D_h are both sized $2n_x(n_x-1) \times 2n_x(n_x-1)$. Furthermore, the matrix $K_h^* K_h$ is the symmetric positive semi-definite (SPD), and K_h is the block Toeplitz having Toeplitz blocks (BTTB) matrix. The arrangement of matrix B_h can be represented as:

$$B_h = \frac{1}{h} \begin{bmatrix} B_1 \\ B_2 \end{bmatrix}$$

here B_1 and B_2 are $n_x(n_x-1) \times n_x^2$ in size.

$$B_1 = C \otimes I, \qquad B_2 = I \otimes C.$$

The matrix

$$C = \begin{bmatrix} 1 & -1 & & & & \\ & 1 & -1 & & & \\ & & \ddots & \ddots & & \\ & & & \ddots & -1 & \\ & & & & 1 & -1 \end{bmatrix},$$

has dimensions $(n_x-1) \times n_x$, and I represents the identity matrix. On the other hand, matrix D_h is the diagonal, with its entries derived from discretizing the expression $\sqrt{|\bigtriangledown k|^2 + \beta^2}$. Importantly, all the entries of D_h are positive.

$$D_h(U) = \begin{bmatrix} D^x & 0 \\ 0 & D^y \end{bmatrix},$$

here D^x having size $(n_x-1) \times n_x$, and D^y having size $n_x \times (n_x-1)$. The matrix is also a diagonal matrix.

$$G_h(U) = \begin{bmatrix} G^x & 0 \\ 0 & G^y \end{bmatrix}.$$

The entries of the matrix can be obtained through discretizing the expression $\bigtriangledown \kappa . \frac{\bigtriangledown k}{\sqrt{|\bigtriangledown k|^2 + \beta^2}}$. The matrix G^x having size $(n_x-1) \times n_x$, and matrix G^y having size $n_x \times (n_x-1)$. To calculate the value of k, one has to resolve Equation (33). Concerning the Lagrange multipliers and remaining variables, a direct solution method is employed after discretization on grid points (i, j). So from Equation (17), we have

$$w^*(i,j) = \max\{0,\ u(i,j) - \lambda_1(i,j)/c - a_1\}. \quad (34)$$

To update Lagrange multiplier, we need the following equations:

$$\lambda_1^{(n+1)}(i,j) = \lambda_1^{(n)}(i,j) + c^{(n)} \max\{-k^{(n)}(i,j), \lambda_1^{(n)}/c^{(n)}\} \tag{35}$$

$$\lambda_2^{(n+1)}(i,j) = \lambda_2^{(n)}(i,j) + c^{(n)}(k^{(n)}(i,j) - \frac{1}{\mid \Omega \mid}) \tag{36}$$

$$\lambda_3^{(n+1)}(i,j) = \lambda_3^{(n)}(i,j) + c^{(n)}(k(x,y) - k(-x,-y)) \tag{37}$$

3.2. Discretization of image minimization problem

The CCFD approximations $\{U_{i,j}\}$ to $\{u(x_{i,j})\}$ and $\{K_{i,j}\}$ to $\{k(x_{i,j})\}$ are chosen. So from Equation (25), we have

$$\begin{aligned}&[K^*KU]_{i,j} + \alpha_1[div^-(\frac{\bigtriangledown^+\kappa}{\sqrt{[\bigtriangledown^+U]_{i,j}^2 + \beta^2}} - \frac{\bigtriangledown^+\kappa.\ \bigtriangledown^+U}{(\sqrt{[\bigtriangledown^+U]_{i,j}^2 + \beta^2})^3}\ \bigtriangledown^+U)]_{i,j} + cU_{i,j} \\ &= [K^*Z]_{i,j}.\end{aligned} \tag{38}$$

The Euler-Lagrange equation of the image minimization problem is quite similar to the Euler-Lagrange equation of the kernel minimization problem. The only difference is the underlying variable. That is why, by using lexicographical ordering of the unknowns, $U = [U_{11} \quad U_{12} \quad ... \quad U_{n_xn_x}]^t$ and $K = [K_{11} \quad K_{12} \quad ... \quad K_{n_xn_x}]^t$, we have the following similar matrix system:

$$(K_h^*K_h + \alpha_1(B_h^*D_h^{-1}(U)B_h)^2 + \alpha_1 B_h^*D_h^{-1}(U)G_h(U)D_h^{-1}B_h + cI)U = K_h^*Z. \tag{39}$$

To calculate the value of u, one needs to resolve Equation (39). For the remaining variables and the Lagrange multipliers, a direct solution method is employed after discretization on grid points (i,j). So from Equations (28) and (29), we have

$$w_1^*(i,j) = \max\{0,\ u(i,j) - \lambda_1(i,j)/c - a_1\}, \tag{40}$$

$$w_2^*(i,j) = \max\{0,\ -u(i,j) - \lambda_2(i,j)/c + a_2\}. \tag{41}$$

To update the Lagrange multiplier, we need the following equations:

$$\lambda_1^{(n+1)}(i,j) = \lambda_1^{(n)}(i,j) + c^{(n)} \max\{-u^{(n)}(i,j),\ -\lambda_1^{(n)}(i,j)/c^{(n)} - a_1\} \tag{42}$$

$$\lambda_2^{(n+1)}(i,j) = \lambda_2^{(n)}(i,j) + c^{(n)} \max\{u^{(n)}(i,j),\ -\lambda_2^{(n)}(i,j)/c^{(n)} + a_2\}. \tag{43}$$

Both Equations (33) and (39) are nonlinear positive definite symmetric systems. So one can first use the fixed point iteration (FPI) method [30] or Newton's method [31] to linearize them. Subsequently, the conjugate gradient (CG) method is utilized to obtain the solution.

4. Numerical experiments

In this section, our algorithms are applied to address image deblurring issues. Multiple sets of experiments are conducted using various digital images. The algorithms are executed using MATLAB, and all computational experiments are conducted on an Intel® Core™ i7-4510U CPU (2.60 GHz). The quality of restored image is assessed using two metrics: peak signal-to-noise ratio (PSNR) and structure

similarity index measure (SSIM). The values for parameters α_1, α_2 and β are determined by referencing the previous works [6–8]. In all experiments, we initialize the guess for the restored image, denoted as u^0 with the blurred data z. Different values of n_x are employed, leading to a matrix system with n_x^2 unknowns. The size of the mesh is determined as $h = 1/n_x$. Throughout of the experiments, the numerical iterations are terminated when the residuals satisfy the condition $\|b - Ax^n\| < tol \parallel b \parallel$, where x^n represents solution vector at m-th iteration. The outcomes are given in the tables and figures below.

Example 1. *In this instance, we utilized the test images dataset of Levin et al. [32]. The 4 images and 8 different blur kernels of Levin et al.'s [32] data set are shown in* ***Figure 2****. To produce blurry images, all sharp images are affected by individual blur kernels and additive white Gaussian noise with a standard deviation of* $\sigma = 0.01$*. So one can get 32 degraded images for testing. In this experiment, we conducted a comparative analysis between our proposed MBD method and several existing methods for solving BID problems. For conducting the comparison, we utilised the Bayesian blind deconvolution (BBD) method [33], the deblurring with directional filters (DDF) method [34], the normalized sparsity measure (NSM) technique [35], and* L_0- *regularized intensity and gradient prior (L0RIG) technique [36]. Recovered images of kids of size* 255×255 *presented in* ***Figure 3****. Calculated kernels of each method are also shown in* ***Figure 3****. In MBD method, the problem was solved with the help of PGMRES technique while incorporating the MC regularization functional alongside specified parameters* $\alpha_1 = 1 \times 10^{-7}, \alpha_2 = 1 \times 10^{-13}, \beta = 0.4$*.* ***Table 1*** *shows PSNR and SSIM information of different techniques on kids' image. Mean PSNR and mean SSIM results of different methods on dataset of Levin et al. [32] are depicted in* ***Figure 4****.*

Figure 2. The images and blur kernels of dataset of Levin et al. [32].

(a) **(b)** **(c)**

Figure 3. *Cont.*

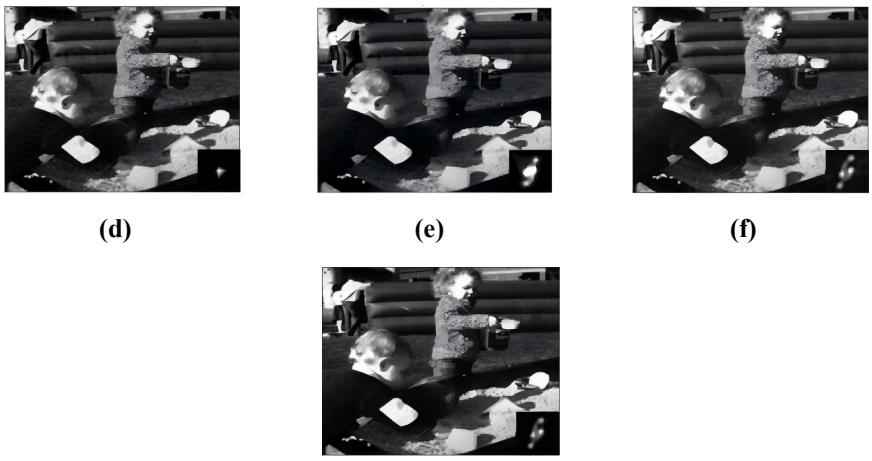

(d) **(e)** **(f)**

(g)

Figure 3. Kids' image: **(a)** Exact image, **(b)** blurred image, **(c)** deblurred using BBD method, **(d)** deblurred using DDF method, **(e)** deblurred image using NSM method, **(f)** deblurred image using L0RIG method and **(g)** deblurred image using BDM method.
Note: The estimated kernels are on the bottom right corners.

Table 1. PSNR and SSIM comparison kids' image.

Method	PSNR	SSIM
Blurred	15.2564	0.6126
TV	23.8769	0.7567
BBD	28.3975	0.8480
NSM	22.7151	0.7568
DDF	24.9047	0.7647
L0RIG	25.8597	0.8125
MBD	28.9946	0.8566

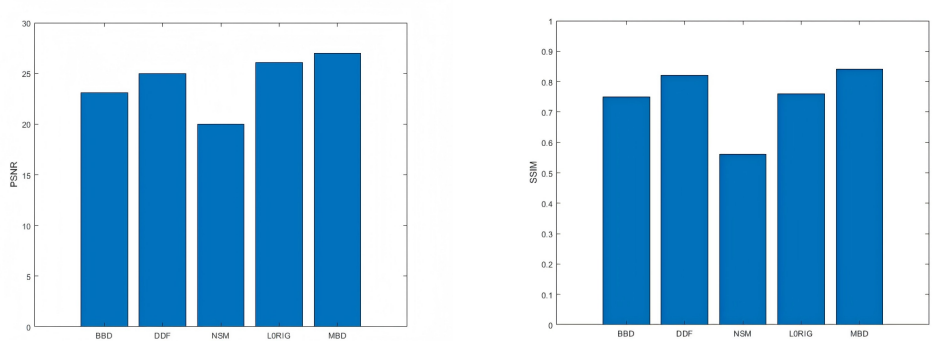

(a) **(b)**

Figure 4. **(a)** Mean PSNR and **(b)** mean SSIM results of different methods on dataset of Levin et al. [32].

Remark 1. *By observing **Figure 3**, with a necked eye it is difficult to understand which method is performing well. Its look all method are generating the same quality images. But it is clearly seen that BBD, L0RIG and MBD methods are giving better estimates for kernel. Further investigation can be made with PSNR and SSIM.*

*From **Table 1**, it is evident that MBD technique is getting high PSNR and SSIM as compared to all existing methods. So our proposed method is performing better. This can also be observed from **Figure 4** in which mean PSNR and mean SSIM of all methods are depicted. The mean value of our MBD method is also higher than that of all other*

methods for both PSNR and SSIM measures.

Example 2. *In this example we used three benchmark images from literature. These are a Cameraman, Goldhills and Peppers images. The image of Cameraman is challenging because it combines a large-scale cartoon element (face) with a texture on a small scale (the shirt). Image of Goldhills is a real image and image of peppers is a non-texture image. In this experiment, we used images of size* 256×256 *and we employed a motion blur kernel having a size of* 64×64 *to induce blurring in the image. In the noisy image, we introduced Gaussian noise having mean (*μ*) of 0.1 and a standard deviation (*σ^2*) of 1.01. Dealing with blurred images that are degraded by motion blur kernels poses a significant challenge for most deblurring methods. This is primarily due to the presence of saturated pixels, which can hinder the accurate estimation of the blur kernel. To facilitate comparison, we have employed the OLM, TLM and OSCM, TSCM [37] methods. The restored images can be observed in the* ***Figures 5–7****. While the calculated kernels are displayed in* ***Figure 8****. In the MBD method, we have used parameters* $\alpha_1 = 1 \times 10^{-9}, \alpha_2 = 1 \times 10^{-10}, \beta = 0.01$. ***Table 2*** *shows PSNR and SSIM details about this experiment.*

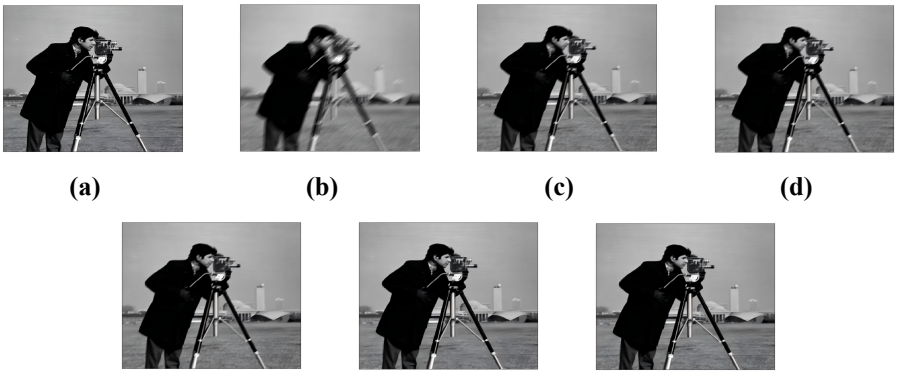

(a) **(b)** **(c)** **(d)**

(e) **(f)** **(g)**

Figure 5. Cameraman image: **(a)** exact image, **(b)** blurry image, **(c)** deblurred image using OSCM technique, **(d)** deblurred image using TSCM technique, **(e)** deblurred image using OLM technique, **(f)** deblurred image using TLM technique and **(g)** deblurred image using MBD technique.

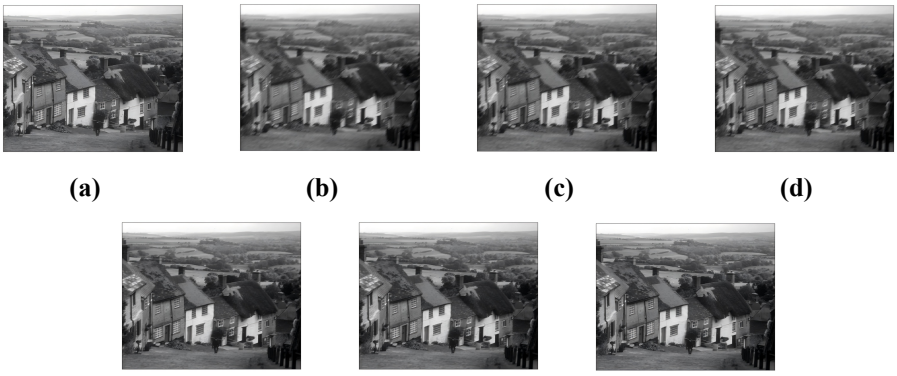

(a) **(b)** **(c)** **(d)**

(e) **(f)** **(g)**

Figure 6. Goldhills image: **(a)** exact image, **(b)** blurry image, **(c)** deblurred image using OSCM technique, **(d)** deblurred image using TSCM technique, **(e)** deblurred image using OLM technique, **(f)** deblurred image using TLM technique and **(g)** deblurred image using MBD technique.

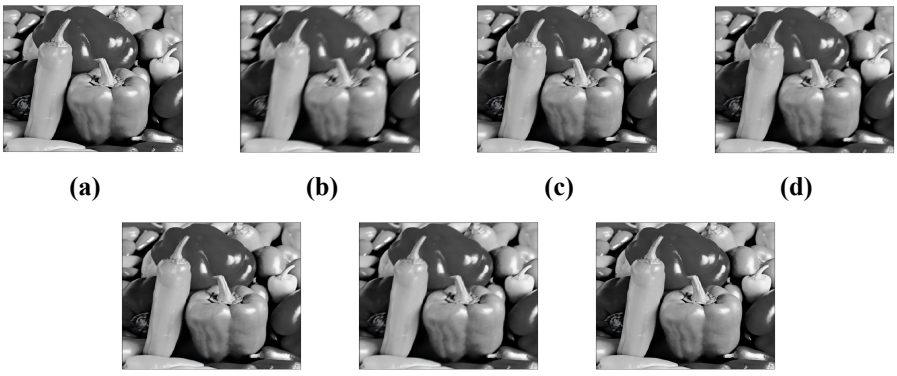

(a) **(b)** **(c)** **(d)**

(e) **(f)** **(g)**

Figure 7. Peppers image: **(a)** exact image, **(b)** blurry image, **(c)** deblurred image using OSCM technique, **(d)** deblurred image using TSCM technique, **(e)** deblurred image using OLM technique, **(f)** deblurred image using TLM technique and **(g)** deblurred image using MBD technique.

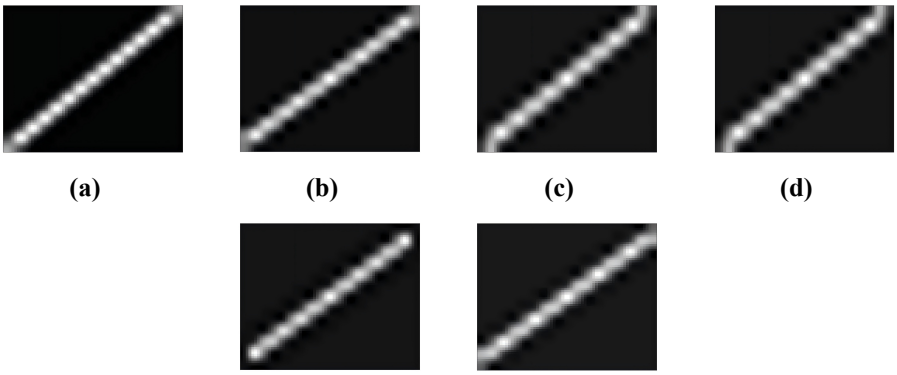

(a) **(b)** **(c)** **(d)**

(e) **(f)**

Figure 8. **(a)** Exact kernel, **(b)** estimated kernel using OSCM technique, **(c)** estimated kernel using TSCM technique, **(d)** estimated kernel using OLM technique, **(e)** estimated kernel using TLM technique and **(f)** estimated kernel using MBD technique.

Table 2. PSNR, SSIM and CPU-Time comparison for Example 2.

Method		**Blurred**	**OSCM**	**TSCM**	**OLM**	**TLM**	**MBD**
Cameraman	PSNR	23.9379	46.3645	45.5634	43.1548	43.3441	46.7679
	SSIM	0.7524	0.9186	0.9121	0.7047	0.9113	0.9233
	CPU-Time		512.3641	526.3428	592.3464	345.2675	442.3453
Goldhills	PSNR	23.1246	34.0517	34.1985	33.6871	33.5241	34.0101
	SSIM	0.6480	0.9133	0.9126	0.9215	0.9405	0.9401
	CPU-Time		896.4058	909.5469	1005.3464	726.5476	912.2343
Peppers	PSNR	23.1569	46.1376	46.5421	45.3434	45.2744	46.9058
	SSIM	0.7103	0.8438	0.8442	0.8595	0.8425	0.9513
	CPU-Time		764.5225	791.2988	880.2645	524.7881	795.8454

Remark 2. *From **Figures 5–7** and **Table 2**, one can observe that our proposed MBD technique is generating much better PSNR and SSIM values compared to all existing techniques. Although the MBD method takes a slightly higher CPU time, but generating high quality as compared to all other methods. The estimated kernels in **Figure 8** are almost the same for all techniques. So the deblurred image quality of the MBD technique is better than that of other techniques.*

5. Conclusion

The manuscript presents a novel iterative approach for addressing blind image deblurring problems. The proposed method aims to restore blurred images without prior knowledge or with some partial information of the blur kernel, which is a challenging task in image processing. Throughout the manuscript, various sets of experiments were conducted using distinct digital images to evaluate the effectiveness of the algorithm. The results obtained from the experiments demonstrate the capability of the proposed method in restoring images degraded by different blur kernels. Compared to existing methods such as OSCM, TSCM, OLM, TLM, BBD, DDF, NSM, and L0RIG, the new iterative approach shows promising performance in terms of image restoration. Overall, the manuscript contributes to the field of blind image deblurring by introducing a new iterative method and providing comprehensive experimental results. The proposed approach shows potential for improving image restoration in scenarios where blur kernels are unknown, thus enhancing the overall image quality and enabling further applications in areas such as computer vision and image analysis. In future work, we plan to extend our approach to RGB and multispectral images by incorporating suitable regularization strategies that enforce inter-channel consistency.

Author contributions: Conceptualization, SA and AMAM; methodology, SS and AI; software, AI and FF; validation, FF and SA; formal analysis, AI and SA; investigation, SS and AI; writing—original draft preparation, AI and SA; writing—review and editing, SA and SS; visualization, AI; supervision, SA; project administration, AI; funding acquisition, AI. All authors have read and agreed to the published version of the manuscript.

Funding: This work received no external funding.

Institutional review board statement: Not applicable.

Informed consent statement: Not applicable.

Data availability statement: The data that support the findings of this study are available from the corresponding author upon reasonable request.

Conflict of interest: There is no conflict of interest, according to the authors.

AI use statement: The authors declare that no artificial intelligence (AI) tools were used in the preparation of this manuscript.

References

1. Xu H, Li F. Smoothing Priors for Blind Image Deblurring. SIAM Journal on Imaging Sciences. 2025; 18(1): 216–245.
2. Choi NR. A Comparative Study of Non-Blind and Blind Deconvolution of Ultrasound Images. University of Southern California; 2014.
3. Tao S, Dong W, Feng H, et al. Non-blind image deconvolution using natural image gradient prior. Optik. 2013; 124(24): 6599–6605.
4. Xiong N, Liu RW, Liang M, et al. Effective alternating direction optimization methods for sparsity-constrained blind image deblurring. Sensors. 2017; 17(1): 174.
5. Inampudi S, Vani S, TB R. Image Restoration using Non-Blind Deconvolution Approach–A Comparison.

International Journal of Electronics and Communication Engineering and Technology. 2019; 10(1).
6. Campisi P, Egiazarian K. Blind Image Deconvolution: Theory and Applications. CRC Press; 2016.
7. Ge X, Tan J, Zhang L, et al. Blind image deblurring with Gaussian curvature of the image surface. Signal Processing: Image Communication. 2022; 100: 116531.
8. Li L, Pan J, Lai WS, et al. Learning a discriminative prior for blind image deblurring. In: Proceedings of the IEEE Conference on Computer Vision and Pattern Recognition; 18–23 June 2018; Salt Lake City, UT, USA. pp. 6616–6625.
9. Chen K. Introduction to variational image-processing models and applications. International Journal of Computer Mathematics. 2013; 90(1): 1–8.
10. Yang F, Chen K, Yu B, et al. A relaxed fixed point method for a mean curvature-based denoising model. Optimization Methods and Software. 2014; 29(2): 274–285.
11. Mobeen A, Ahmad S, Fairag F. Non-blind constraint image deblurring problem with mean curvature functional. Numerical Algorithms. 2025; 98(4): 1703–1723.
12. Peng J, Luo B, Xu L, et al. Blind image deblurring via minimizing similarity between fuzzy sets on image pixels. IEEE Transactions on Circuits and Systems for Video Technology. 2024; 34(11): 11851–11873.
13. Kim K, Lee Y. Investigation of Blind Deconvolution Method with Total Variation Regularization in Cardiac Cine Magnetic Resonance Imaging. Electronics. 2025; 14(4): 743.
14. El Mourabit I, El Rhabi M, Hakim A. Blind deconvolution using bilateral total variation regularization: a theoretical study and application. Applicable Analysis. 2022; 101(16): 5660–5673.
15. Chan TF, Wong CK. Total variation blind deconvolution. IEEE transactions on Image Processing. 1998; 7(3): 370–375.
16. Zhang J, Deng C, Shi Y, et al. A fast linearised augmented Lagrangian method for a mean curvature based model. East Asian Journal on Applied Mathematics. 2018; 8(3): 463–476.
17. Zhu W, Chan T. Image denoising using mean curvature of image surface. SIAM Journal on Imaging Sciences. 2012; 5(1): 1–32.
18. Bardsley JM, Vogel CR. A nonnegatively constrained convex programming method for image reconstruction. SIAM Journal on Scientific Computing. 2004; 25(4): 1326–1343.
19. Calvetti D, Landi G, Reichel L, et al. Non-negativity and iterative methods for ill-posed problems. Inverse Problems. 2004; 20(6): 1747.
20. Benvenuto F, Zanella R, Zanni L, et al. Nonnegative least-squares image deblurring: improved gradient projection approaches. Inverse Problems. 2009; 26(2): 025004.
21. Chan RH, Tao M, Yuan X. Constrained total variation deblurring models and fast algorithms based on alternating direction method of multipliers. SIAM Journal on imaging Sciences. 2013; 6(1): 680–697.
22. Williams BM, Chen K, Harding SP. A new constrained total variational deblurring model and its fast algorithm. Numerical Algorithms. 2015; 69(2): 415–441.
23. Tai XC, Hahn J, Chung GJ. A fast algorithm for Euler's elastica model using augmented Lagrangian method. SIAM Journal on Imaging Sciences. 2011; 4(1): 313–344.
24. Wu C, Tai XC. Augmented Lagrangian method, dual methods, and split Bregman iteration for ROF, vectorial TV, and high order models. SIAM Journal on Imaging Sciences. 2010; 3(3): 300–339.
25. Chan SH, Khoshabeh R, Gibson KB, et al. An augmented Lagrangian method for total variation video restoration. IEEE Transactions on Image Processing. 2011; 20(11): 3097–3111.
26. Iqbal A, Ahmad S, Kim J. Two-Level method for blind image deblurring problems. Applied Mathematics and Computation. 2025; 485: 129008.
27. Khalid R, Ahmad S, Ali I, et al. Enhanced BiCGSTAB with Restrictive Preconditioning for Nonlinear Systems: A Mean Curvature Image Deblurring Approach. Mathematical and Computational Applications. 2025; 30(4): 76.
28. Liu H, Sun J, Liu J, et al. Blind Noisy Image Deblurring Using Residual Guidance Strategy. In: Proceedings of the IEEE/CVF International Conference on Computer Vision; 19–25 October 2025; Honolulu, HI, USA. pp. 11016–11025.
29. Wu C, Zhang L, Zhang T, et al. Total curvature-driven blind image deblurring. Journal of Computational and Applied Mathematics. 2025; 117089.
30. Vogel CR, Oman ME. Fast, robust total variation-based reconstruction of noisy, blurred images. IEEE Transactions on Image Processing. 1998; 7(6): 813–824.
31. Landi G, Loli Piccolomini E. A projected Newton-CG method for nonnegative astronomical image deblurring.

Numerical Algorithms. 2008; 48(4): 279–300.
32. Levin A, Weiss Y, Durand F, et al. Understanding and evaluating blind deconvolution algorithms. In: Proceedings of the 2009 IEEE Conference on Computer Vision and Pattern Recognition; 20–25 June 2009; Miami, FL, USA. pp. 1964–1971.
33. Babacan SD, Molina R, Do MN, et al. Bayesian blind deconvolution with general sparse image priors. In: Proceedings of the Computer Vision–ECCV 2012: 12th European Conference on Computer Vision; 7–13 October 2012; Florence, Italy. pp. 341–355.
34. Zhong L, Cho S, Metaxas D, et al. Handling noise in single image deblurring using directional filters. In: Proceedings of the IEEE Conference on Computer Vision and Pattern Recognition; 23–28 June 2013; Portland, OR, USA. pp. 612–619.
35. Krishnan D, Tay T, Fergus R. Blind deconvolution using a normalized sparsity measure. In: Proceedings of the CVPR 2011; 20–25 June 2011; Colorado Springs, CO, USA. pp. 233–240.
36. Pan J, Hu Z, Su Z, et al. l_0 -regularized intensity and gradient prior for deblurring text images and beyond. IEEE Transactions on Pattern Analysis and Machine Intelligence. 2016; 39(2): 342–355.
37. Saleem S, Ahmad S, Kim J. Total fractional-order variation-based constraint image deblurring problem. Mathematics. 2023; 11(13): 2869.